frontiers | Frontiers in Cell and Developmental Biology

TYPE Original Research
PUBLISHED 28 May 2024
DOI 10.3389/fcell.2024.1382960



OPEN ACCESS

EDITED BY
Aimin Liu,
The Pennsylvania State University (PSU), United States

REVIEWED BY
Tae Hyun Kim,
The Pennsylvania State University (PSU), United States
Peng-Fei Xu,
Zhejiang University, China
Amanda Janesick,
10x Genomics, United States

*CORRESPONDENCE
G. F. Mok,
g.mok@uea.ac.uk
I. C. Macaulay,
iain.macaulay@earlham.ac.uk
A. E. Münsterberg,
a.munsterberg@uea.ac.uk

†PRESENT ADDRESSES
S. Turner, Department of Zoology, University of Cambridge, Cambridge, United Kingdom
L. Mincarelli and V. Uzun, Wellcome Sanger Institute, Wellcome Trust Genome Campus, Saffron Walden, United Kingdom

RECEIVED 06 February 2024
ACCEPTED 29 April 2024
PUBLISHED 28 May 2024

CITATION
Mok GF, Turner S, Smith EL, Mincarelli L, Lister A, Lipscombe J, Uzun V, Haerty W, Macaulay IC and Münsterberg AE (2024), Single cell RNA-sequencing and RNA-tomography of the avian embryo extending body axis.
*Front. Cell Dev. Biol.* 12:1382960.
doi: 10.3389/fcell.2024.1382960



# Single cell RNA-sequencing and RNA-tomography of the avian embryo extending body axis

G. F. Mok[1]*, S. Turner[2†], E. L. Smith[1], L. Mincarelli[2†], A. Lister[2], J. Lipscombe[2], V. Uzun[2†], W. Haerty[2], I. C. Macaulay[2]* and A. E. Münsterberg[1]*

[1]School of Biological Sciences, University of East Anglia, Norwich, United Kingdom, [2]Earlham Institute, Norwich, United Kingdom

**Introduction:** Vertebrate body axis formation initiates during gastrulation and continues within the tail bud at the posterior end of the embryo. Major structures in the trunk are paired somites, which generate the musculoskeletal system, the spinal cord—forming part of the central nervous system, and the notochord, with important patterning functions. The specification of these different cell lineages by key signalling pathways and transcription factors is essential, however, a global map of cell types and expressed genes in the avian trunk is missing.

**Methods:** Here we use high-throughput sequencing approaches to generate a molecular map of the emerging trunk and tailbud in the chick embryo.

**Results and Discussion:** Single cell RNA-sequencing (scRNA-seq) identifies discrete cell lineages including somites, neural tube, neural crest, lateral plate mesoderm, ectoderm, endothelial and blood progenitors. In addition, RNA-seq of sequential tissue sections (RNA-tomography) provides a spatially resolved, genome-wide expression dataset for the avian tailbud and emerging body, comparable to other model systems. Combining the single cell and RNA-tomography datasets, we identify spatially restricted genes, focusing on somites and early myoblasts. Thus, this high-resolution transcriptome map incorporating cell types in the embryonic trunk can expose molecular pathways involved in body axis development.

KEYWORDS

**chick embryo, axis extension, somites, single cell RNA-sequencing, RNA-tomography**

## Introduction

The generation of somites, which arise in a regular sequence during embryogenesis, is fundamental for creating the vertebrate segmented body plan (Benazeraf and Pourquie, 2013). Pairs of somites form on either side of the neural tube from unsegmented, paraxial mesoderm, and the process of somitogenesis, which involves waves of cycling gene expression, has been studied extensively in chick embryos (Pourquie, 2004). Prospective paraxial mesoderm cells emerge from the primitive streak during gastrulation (Psychoyos and Stern, 1996) and follow a stereotypical migration trajectory towards their destination (Yang et al., 2002; Iimura et al., 2007). As the body axis elongates, bi-potential neuromesodermal progenitors (NMP) located in the tailbud continue to generate paraxial mesoderm and cells of the neural tube (Wilson et al., 2009; Henrique et al., 2015; Wymeersch et al., 2021). The dynamics of this specialised cell population has been

mapped in detail in chick embryos (Guillot et al., 2021) and it has been shown that the extension of neural and paraxial mesoderm tissues in the embryonic body is coordinated by mechanical interactions (Xiong et al., 2020).

Somite differentiation proceeds along the posterior-to-anterior axis and serves as a paradigm for the study of cell fate specification. Multiple signals from surrounding tissues are integrated by somite cells to produce the lineages of the musculoskeletal system, including chondrocytes of the axial skeleton and skeletal muscles of the trunk and limbs (Brent and Tabin, 2002; Christ et al., 2007; Christ and Scaal, 2008). Cell fate specification is intimately linked to stereotypic morphological changes resulting in somite compartmentalisation. For example, tracking of GFP-labelled cells showed that the dorsal dermomyotome produces the myotome layer in multiple waves, with the first myocytes specified adjacent to the neural tube (Gros et al., 2004). Live-imaging of cellular rearrangements examined the morphological transformations of somites, from epithelial structures to somites with a mesenchymal sclerotome, located ventrally, and an epaxial myotome abutting the neural tube (McColl et al., 2018). This uncovered differential cell sizes and regions of proliferation as well as a directed movement of dermomyotomal progenitor cells towards the rostro-medial domain of the dermomyotome, where skeletal muscle formation initiates.

To better characterise the regulation of these morphogenetic events and their integration with cell specification and differentiation, we previously used bulk sequencing to assess the dynamic changes of the transcriptome and of chromatin accessibility across presegmented mesoderm and early, maturing and differentiating somites (Mok et al., 2021). Associating differentially accessible chromatin with nearby genes, differentially expressed along the axis, identified candidate cis-regulatory elements (CREs) involved in expression of transcription factors important for somite formation and differentiation. Time-lapse microscopy in accessible chick embryos of fluorescent CRE-reporters revealed their spatio-temporal activity, and mutation analysis uncovered some upstream regulators. Similarly in mice, we examined matched gene expression and open chromatin profiles for newly formed somite pairs across a developmental time series. This provided a high-resolution view of the molecular signatures underlying the conserved maturation programme followed by all somites after segmentation (Ibarra-Soria et al., 2023).

Here we focus on the initial phase of trunk development in chick embryos. This complements recent *in vitro* organoid models of axis elongation, which are based on the differentiation of mouse or human pluripotent stem cells and use pharmacological activation or inhibition of crucial signalling pathways (Veenvliet and Herrmann, 2021). These protocols generate self-organising structures including gastruloids (Turner et al., 2017; Moris et al., 2020), trunk-like structures (Veenvliet et al., 2020), somitoids (Sanaki-Matsumiya et al., 2022), or axioloids (Yamanaka et al., 2023). These structures often comprise mesoderm, including somites, although the notochord, which is involved in patterning of trunk tissues, is missing. Thus, it is important to reconstruct the molecular profiles and cellular composition in the native tissues.

Here, we use single cell transcriptomics combined with an RNA-tomography based approach, analogous to Tomo-seq (Junker et al., 2014; Kruse et al., 2016) but using a modified G&T-seq approach (Macaulay et al., 2015). This generated a spatio-temporal map of the emerging trunk and identified genes not previously known to be involved in pre-somitic/pre-segmented mesoderm (psm) and somite maturation. Our study complements data in chick embryos, from earlier developmental stages (HH4-HH11) (Vermillion et al., 2018; Williams et al., 2022; Rito et al., 2023), from tailbud (Guillot et al., 2021) and from prospective neural plate, neural plate border and non-neural ectoderm (Trevers et al., 2023). The dataset is relevant for cell type specification during early body formation and may provide insights into the molecular genetics that underlie diseases of the musculoskeletal system.

# Results

## Single cell profiling of the developing chick embryonic body

To investigate the molecular basis underpinning somitogenesis and axis elongation of the growing chick body, we mapped the transcriptomes of individual cells at embryonic stage HH14 (Hamburger and Hamilton, 1992) (Figure 1A). This stage embryo has 22 somites, including cervical level somites (6–19) and thoracic level somites (20–22). The unsegmented paraxial mesoderm and tailbud comprise prospective somites of the thoracic, lumbar and sacral regions (Weldon and Munsterberg, 2022). Single cell suspensions from the posterior part of five pooled embryos included the extraembryonic region, tailbud, pre-somitic mesoderm and the most recently formed six somites (Figure 1B). Following enzymatic digestion and mechanical dissociation the suspension was processed using the 10X Genomics Chromium. A total of 6158 cells were sequenced with a median of 517 genes and 900 UMIs per cell.

Unsupervised clustering was used to classify cell populations (Butler et al., 2018). Projection onto UMAP plots revealed 10 separate clusters (Figure 1C). These clusters were characterised by expression of classic marker genes, which assigned cluster identity and tissues. These included for the lateral plate mesoderm (*Prrx1* and *Krt18*) (Bell et al., 2004), for neural cells (*Wnt4* and *Olig2*) (Cauthen et al., 2001; Zhou et al., 2001), for epithelial somites (*Meox1* and *Tcf15*) (Stockdale et al., 2000; Reijntjes et al., 2007; Berti et al., 2015), for maturing somite (*Nkx3-2* and *Twist1*) (Nielsen et al., 2001; Tavares et al., 2001), for ectoderm (*Fabp3* and *Wnt6*) (Schubert et al., 2002), for blood (*Hbm* and *Hba1*), for endothelial cells (*Lmo2* and *Sox18*) (Minko et al., 2003; Jaffredo et al., 2005; Javerzat et al., 2009; Anderson et al., 2019), for tailbud/pre-segmented mesoderm (*Cdx4* and *Msgn1*) (Joshi et al., 2019), for notochord (*Tf* and *Shh*) (Lobjois et al., 2004; Yanai et al., 2005) and for neural crest cells (*FoxD3* and *Sox10*) (McKeown et al., 2005) (Figures 1C, D). Seurat cell cycle scoring determined cell cycle activity. This showed overall the cell clustering was not due to cell cycle phase, although neural cells were predominantly in S phase and G2M phase (Figure 1F).

## RNA-tomography profiling of the developing chick embryonic trunk

Spatial information is lost in single cell sequencing data following tissue dissociation (Griffiths et al., 2018). To address

10.3389/fcell.2024.1382960

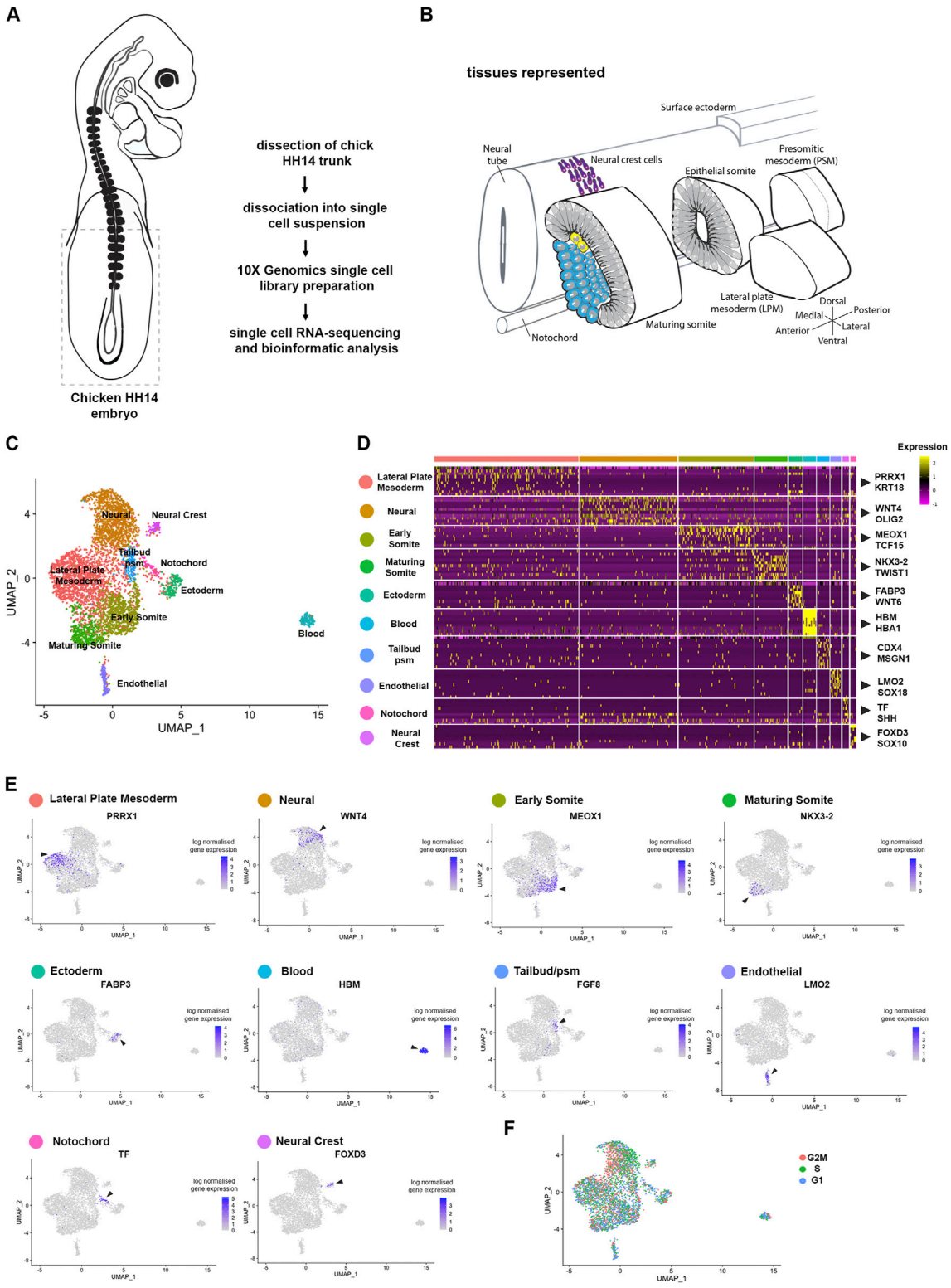


FIGURE 1
Cell population composition and signatures of the HH14 chicken embryo trunk. **(A)** Trunk regions, indicated by stippled lines, of five stage HH14 chicken embryos were collected for scRNA-seq using 10X Genomics Chromium. **(B)** Illustration of developing tissues captured: pre-somitic mesoderm (psm), epithelial somites, maturing somites, lateral plate mesoderm (lpm), surface ectoderm, neural tube and neural crest cells, and notochord. **(C)** Unsupervised UMAP subdivides cells within the trunk into 10 clusters—lateral plate mesoderm, neural progenitors, early somite, maturing somite, pre-somitic mesoderm, ectoderm, blood progenitors, endothelial progenitors and neural crest. **(D)** Heatmap of the top 10 genes significantly enriched in each cluster; representative genes are shown. **(E)** UMAPs show log normalised counts of a representative gene for each cluster. Colour intensity is proportional to expression level of each gene. **(F)** Distribution of cell cycle phases visualised using Seurat cell cycle scoring.

10.3389/fcell.2024.1382960

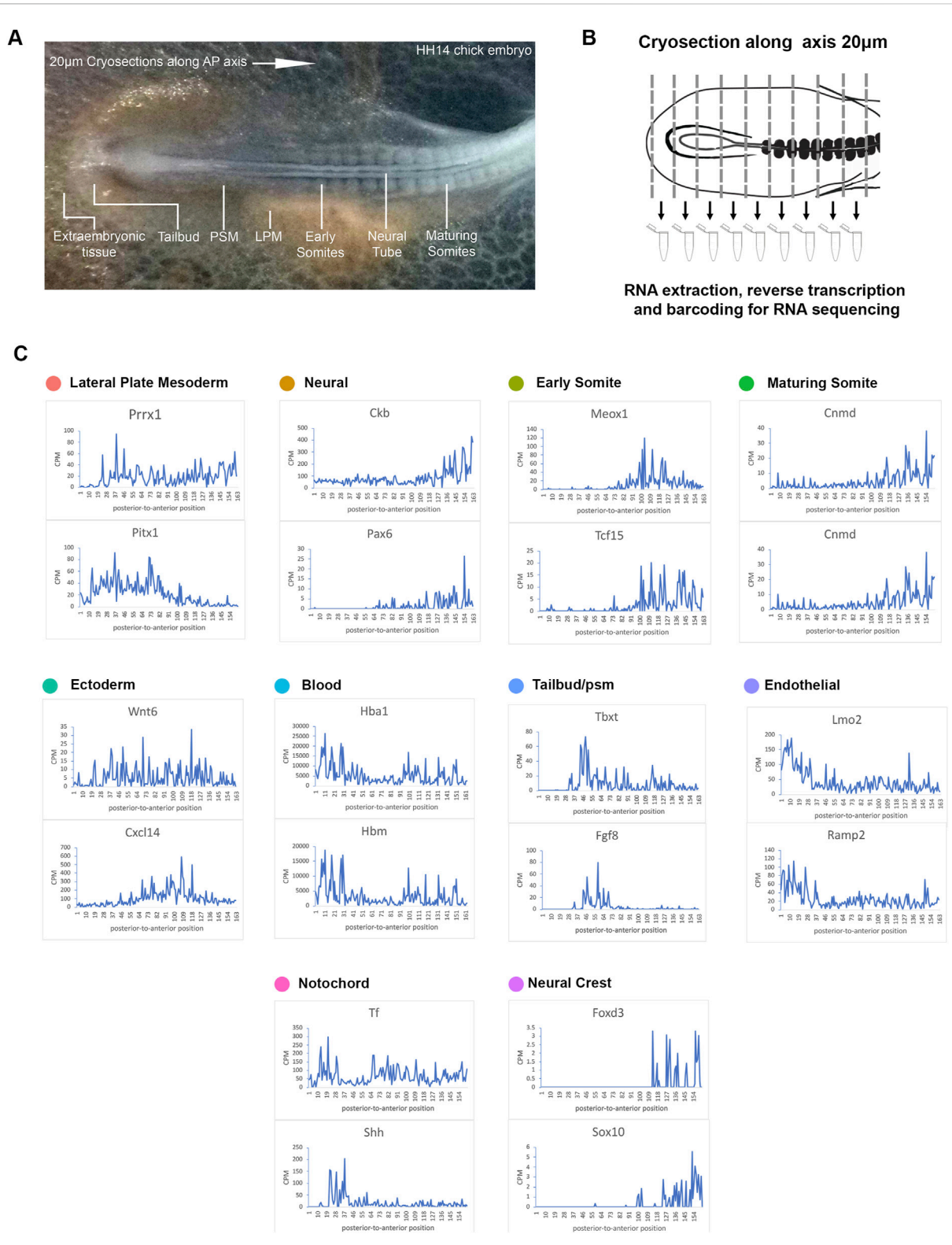


FIGURE 2
RNA-tomography reveals distinct gene expression profiles along the embryonic axis. **(A)** Stage HH14 chick embryo trunk was sectioned along the anterior-to-posterior axis, from extraembryonic tissue at the posterior end, through the tailbud and pre-somitic mesoderm towards maturing somites. **(B)** Individual sections were collected in wells followed by RNA isolation and cDNA preparation using section specific barcodes. After that, samples were pooled for linear amplification and sequence library preparation. **(C)** Spatial expression traces are shown as line plots, left to right represent the posterior to anterior positions. The representative genes shown correspond to the tissue types identified from the scRNA-seq clustering.

10.3389/fcell.2024.1382960

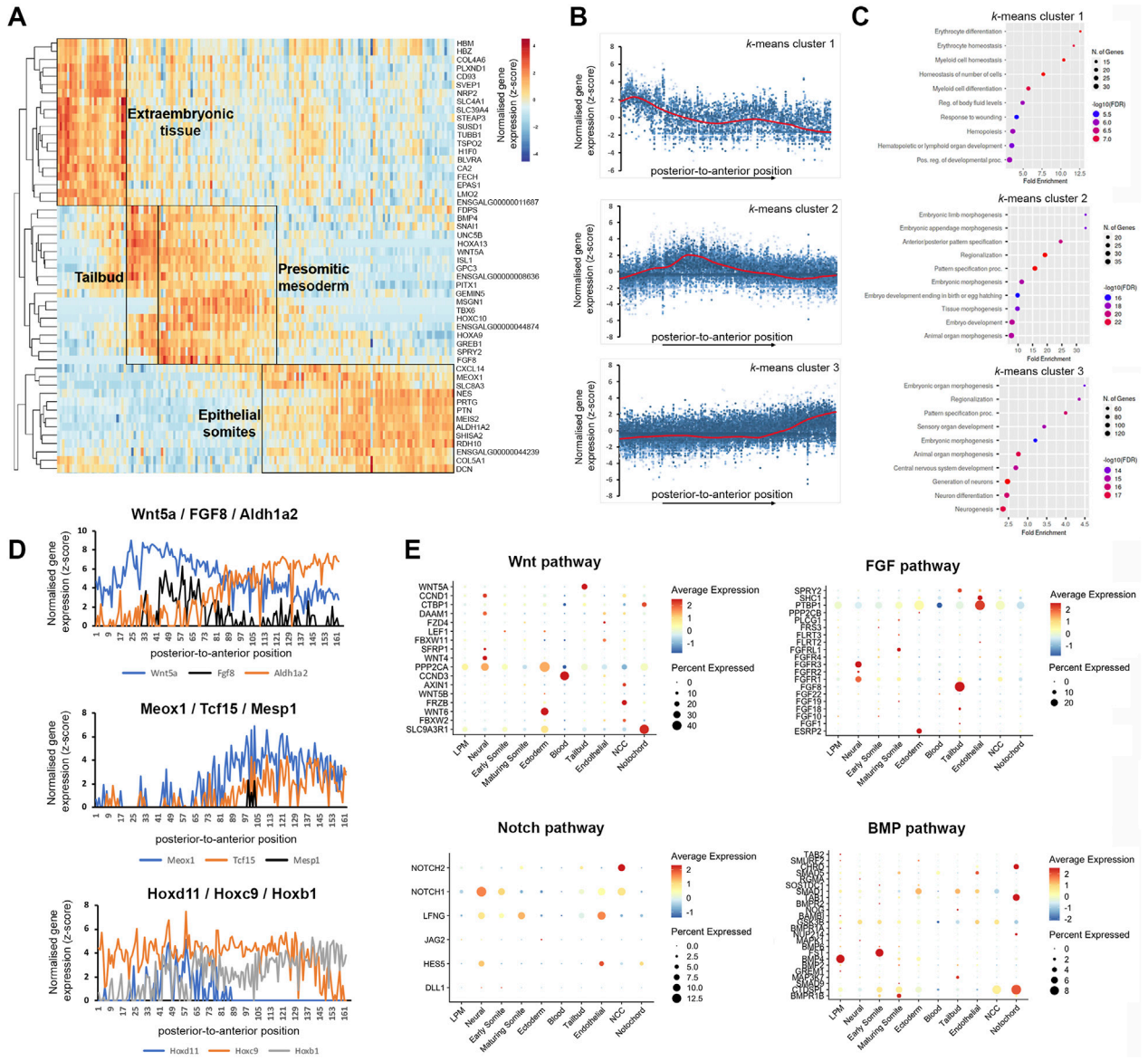


FIGURE 3
K-means clustering identifies biological components along the posterior-to-anterior axis. **(A)** Hierarchical cluster analysis of gene expression per section (total 180). Distinct gene expression clusters correspond to different regions along the axis, characterised by extraembryonic tissue, tailbud, pre-somitic mesoderm and epithelial somites—indicated by boxed areas. RNA sequencing reads per gene were normalised against the total read count per section. **(B)** Spatial expression traces for representative genes in each corresponding cluster, left to right represent the posterior to anterior positions. Cluster 1 represents extraembryonic tissue, cluster 2 tailbud and psm, cluster 3 epithelial somites. **(C)** Gene ontology on genes enriched in the extraembryonic tissue, tailbud and pre-somitic mesoderm, and epithelial somites and neural tube. **(D)** Spatial expression traces for signalling pathways associated with anterior-posterior patterning such as WNT (*Wnt5A*), FGF (*Fgf8*) and retinoic acid (*Aldh1A2*), which are expressed in opposing gradients. Spatial expression traces for genes associated with paraxial mesoderm differentiation (*Meox1*, *Tcf15,* and *Mesp1*), with *Mesp1* highlighting a discreet region in the psm. Spatial expression traces for *Hox* genes involved in anterior-posterior patterning (*Hoxd11*, *Hoxc9,* and *Hoxb1*). Expression of *Hoxd11* and *Hoxc9* displays a clear boundary within the axial region sectioned, while *Hoxb1* expression remains high. Line plots for the other Hox genes are in Supplementary Figure S1. **(E)** Dot plot showing average expression of genes and percentage expressed in each cell cluster associated with the WNT, FGF, NOTCH, and BMP signalling pathways.

this, we next used RNA-tomography to quantify the transcriptomes of a series of individual cryogenic sections along the HH14 embryonic trunk (Figures 2A, B). This enabled a systematic investigation of spatial RNA profiles along the axis and allowed us to resolve the anterior to posterior dimension. Libraries were generated from 20 micron consecutive cryosections of a HH14 chick embryo. Each section was collected into lysis buffer and mRNA captured and amplified using a modification of the G&T-seq protocol (Macaulay et al., 2015). This method allows separating genomic DNA (G) and full-length mRNA (T) from the same sample. Here, we focussed on sequencing transcriptomes. The resulting cDNA libraries had high complexity and enabled us to confidently determine spatial gene expression along the axis (Figure 2C).

Using the same markers as in the previous scRNA-seq analysis (Figures 1C–E), we identified 10 different clusters and established profiles of the lateral plate mesoderm, neural tissue, early somite, maturing somite, ectoderm, blood, endothelial, tailbud, notochord and neural crest cells (Figure 2C). Line graphs indicate spatial patterns of localised anterior-to-posterior restricted gene expression. These were evident for all tissue types with exception of the ectoderm, suggesting that this tissue has few distinguishing markers along the A-P axis. In the most posterior samples, we identified blood *(Hbm*, *Hba1*) and endothelial marker genes (*Lmo2* and *Ramp2*), consistent with this region comprising extra-embryonic tissue (Minko et al., 2003; Jaffredo et al., 2005; Javerzat et al., 2009; Anderson et al., 2019). Subsequent sections showed the onset of tailbud genes [*T* (=*brachyury*) and *Fgf8*] (Dubrulle et al., 2001). Some notochord markers were more highly expressed in posterior sections (*Shh*), while transferrin (*Tf*) was expressed along the axis, with lower levels around the tailbud region (Riddle et al., 1993; Yanai et al., 2005). Across neural tissue (*Ckb*, *Pax6*) (Bhattacharyya et al., 2004; Roy et al., 2013), early somites (*Meox1*, *Tcf15*) (Stockdale et al., 2000; Reijntjes et al., 2007; Berti et al., 2015) and maturing somites (*Cnmd*, *Shisa2*) (Filipe et al., 2006; Shukunami et al., 2008), gene expression profiles showed a gradual increase towards the anterior. Neural crest cells are beginning to migrate and become distinguishable in the more anterior sections with discreet profiles detected for *FoxD3* and *Sox10* (McKeown et al., 2005) (Figure 2C).

## RNA-tomography resolves mRNA localisation patterns

To identify gene expression patterns systematically, we clustered the spatial gene expression data based on a self-organising heatmap. This sorted the cumulative gene expression traces along a linear axis of 180 profiles and identified 3 major groups of localised mRNA (Figure 3A). The first group of transcripts localised to the most posterior, the second group displayed an increase in the tailbud region and across the pre-somitic mesoderm, and the third group was most highly expressed in the anterior sections comprising epithelial and maturing somites (Figure 3B). Transcripts enriched posteriorly (e.g., *Hbm*, *Epas1*, and *Lmo2*) (Minko et al., 2003; Ota et al., 2007; Anderson et al., 2019) were related to Gene Ontology (GO) terms such as hematopoiesis, erythrocyte differentiation and myeloid homeostasis, consistent with the presence of extraembryonic blood islands (Figure 3C). The second profile showed genes enriched for GO processes such as anterior-posterior pattern specification, embryo morphogenesis and tissue morphogenesis. This overlaps spatially with tailbud and pre-somitic regions. Markers with enriched expression included *Wnt5a*, *Msgn1*, *Tbx6,* and *Fgf8* (Dubrulle et al., 2001; Bell et al., 2004; Sweetman et al., 2008) (Figure 3C). The third profile, which overlaps with the formation of somites but also neural tube development, included genes enriched for pattern specification, neurogenesis and animal organ morphogenesis, such as *Meox1, Aldh1a2,* and *Shisa2* (Filipe et al., 2006; Reijntjes et al., 2007) (Figure 3C). Interestingly, the profiles for somites and neural tube are very similar and genes were clustered together, suggesting these tissues mature at a similar rate along the anterior-posterior dimension examined here. However, GO analysis did separate genes associated with generation and differentiation of neurons (Figure 3C). The genes listed for the GO terms, neurogenesis and pattern specification, in *k*-means cluster 3 are shown in Supplementary Table S1. They include neural markers, such as *Wnt4*, *Nkx6.2*, and paraxial mesoderm markers, such as *Meox1*, *Tcf15,* and *Nkx3.2*.

RNA-tomography also detected the known opposing gradients across the psm and somites of *Wnt5a*, *FGF8*, which are increased posteriorly, versus *Aldh1a2*, increasing anteriorly and encoding an enzyme involved in retinoid acid synthesis (Olivera-Martinez and Storey, 2007). This is shown in line graph representation of gene expression along the axis (Figure 3D). The transcripts for *Meox1* and *Tcf15* become upregulated in anterior psm and epithelial somites, whereas *Mesp1* transcripts are restricted to an anterior region in the psm, comprising the next but one prospective somite (Figure 3D). Transcripts for *Hoxd11*, *Hoxc9* and *Hoxb1* show the expected expression boundaries along the anterior-posterior axis (Figure 3D). Line plots for the members of all four Hox clusters, A–D, show the expected expression cut-off along the axis (Supplementary Figure S1). The expression profiles detected by RNA-tomography for anterior Hox gene expression boundaries and epithelial somite marker genes were in agreement with our previous bulk RNA-seq analysis of paraxial mesoderm tissues (Mok et al., 2021).

Furthermore, the spatial resolution provided by the RNA-tomography overlapped with scRNA-seq expression of components of important signalling pathways (Figure 3E). For example, analysis of WNT and FGF pathways, shows high levels of *Wnt5a* and *Fgf8* in tailbud cells, whilst the receptors, *Fgfr1* and *Fgfr3*, were highly expressed in neural cells (Figure 3E). We detected high levels of *Wnt6* in the ectoderm and of Wnt4 in neural cells, consistent with their known expression (Cauthen et al., 2001; Schubert et al., 2002). In addition, the analysis highlighted expression of protein phosphatase, PPP2CA and scaffold protein, SLC9A3R1 in ectodermal cells (Figure 3E). Analysis of NOTCH and BMP pathways confirmed expression of the *Notch1* receptor, the glycosyltransferase, *Lfng*, and the *Hes5* transcription factor in neural cells, while neural crest cells expressed *Notch1* and *Notch2* receptors. The *Bmp4* ligand is highly expressed in the lateral plate, while its antagonists follistatin (*Fst*) and chordin (*Chrd*) are expressed in early somite and notochord respectively. Expression of the receptor, *Bmpr1b* increases in maturing somites (Figure 3E).

## Correlation of single cell RNA-sequencing with RNA-tomography

Axis patterning is characterized by the progressive differentiation of cell types with anterior-to-posterior identity. To validate genes identified in specific clusters obtained from the single cell RNA-sequencing, we correlated spatial patterns and confirmed gene expression by *in situ* hybridisation. This provides a visual point of reference for the tomography sections. Expression of *Hbm*, a haemoglobin gene, is representative for the most posterior group of transcripts, which is enriched for genes involved in hematopoietic differentiation. Consistent with the line graph, we confirm that *Hbm* transcripts are restricted to blood islands in posterior extraembryonic tissue (Figure 4A). The second spatial cluster

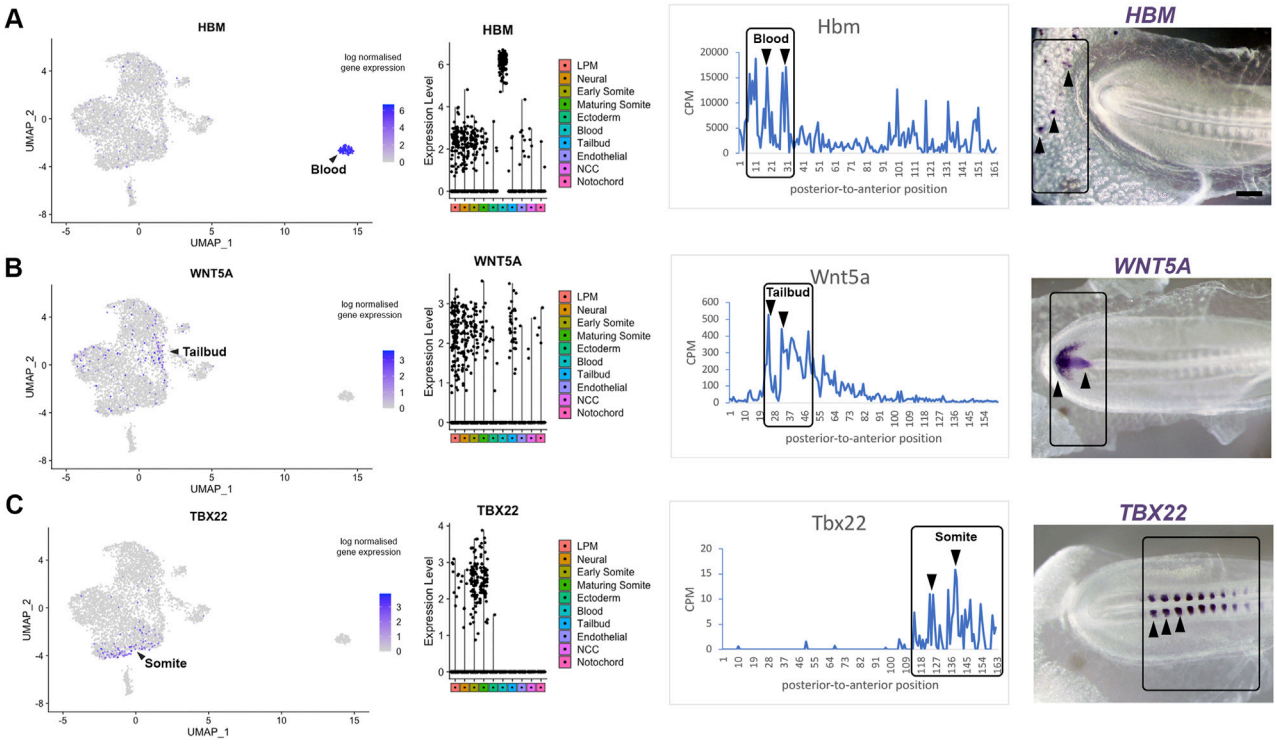


FIGURE 4
Transcriptome map of the embryonic trunk with high spatial resolution. **(A–C)** UMAP plot and violin plot of representative genes for different tissues, with comparison to Spatial expression trace along the posterior-to-anterior axis. The colour coding in the violin plots corresponds to the clusters identified in the scRNA-seq. Corresponding *in situ* hybridisation are shown for **(A)** *Hbm*—blood islands, **(B)** *Wnt5A*—tailbud, **(C)** *Tbx22*—caudal somite halves. This provides a visual point of reference when comparing with the spatial expression along the axis shown by the line plots. See also published gene expression patterns in the data base: http://geisha.arizona.edu/geisha/.

values correlate with the tailbud and pre-somitic mesoderm. We validated this data using *Wnt5a*, which is expressed in the posterior regions at these stages (Baranski et al., 2000) where it regulates cell movement behaviour during axis elongation (Sweetman et al., 2008). *In situ* hybridisation confirmed that *Wnt5a* expression was restricted to the tailbud region (Figure 4B), where neuromesodermal progenitor (NMP) cells are located. The third spatial cluster, where gene expression increased towards the anterior, was validated using *Tbx22*—a key gene for somite boundary formation. Expression of *Tbx22* was restricted to caudal somite domains resulting in an *in situ* signal with periodicity (Figure 4C). All three markers are well characterised (Bell et al., 2004) and help to benchmark the line plots.

## Identification of new genes in paraxial mesoderm and somites

Next, we investigated previously unexplored genes uncovered by our approach. We focused on candidates likely to display restricted expression in the pre-somitic mesoderm and somites. Using the subset feature in Seurat, we profiled three clusters from the scRNA-seq dataset—tailbud, early somite and maturing somite (Figure 5A). We re-ran the clustering, findneighbours and pca tests on this new Seurat object. Classic markers for each cluster were re-plotted on UMAPs, such as *Msgn1* for the pre-somitic mesoderm, *Meox1* and *Tcf15* for early somites and *Tbx22* for maturing somites (Figure 5A). Sub-clustering revealed restricted expression of follistatin (*Fst*), in a group of cells potentially representing myogenic cells located in the dorsal part of epithelial somites (Nimmagadda et al., 2005). We identified three genes for further analysis. UMAP plot of *Olfml3* and *Foxd1* gene expression suggested they are likely to be expressed in maturing somites, whereas *Lrig3* was predicted to be expressed in some pre-somitic mesoderm cells, early somites and less in maturing somites (Figure 5A).

Interrogation of the profiles for these genes in the RNA-tomography data showed that expression of *Foxd1* and *Olfml3* increased towards the anterior regions, with some *Foxd1* expression peaks posteriorly. *Foxd1* and *Olfml3* were identified in spatial cluster 3 (Figure 3). For *Lrig3*, the spatial data showed increasing expression from the most posterior to the anterior embryonic regions, suggesting that it is expressed from the tailbud to maturing somites. Spatial validation for all three genes by *in situ* hybridisation in essence confirmed these observations: *Foxd1* and *Olfml3* are restricted to somites whilst *Lrig3* is expressed in the tailbud, pre-somitic mesoderm and in somites. In epithelial somites, all three genes are restricted medially. In maturing somites *Foxd1* is broadly expressed, *Olfml3* remains medially restricted and *Lrig3* is downregulated (Figures 5B–D). We did not detect any posterior expression of *Foxd1* by *in situ* hybridisation, despite the signal in the line plot.

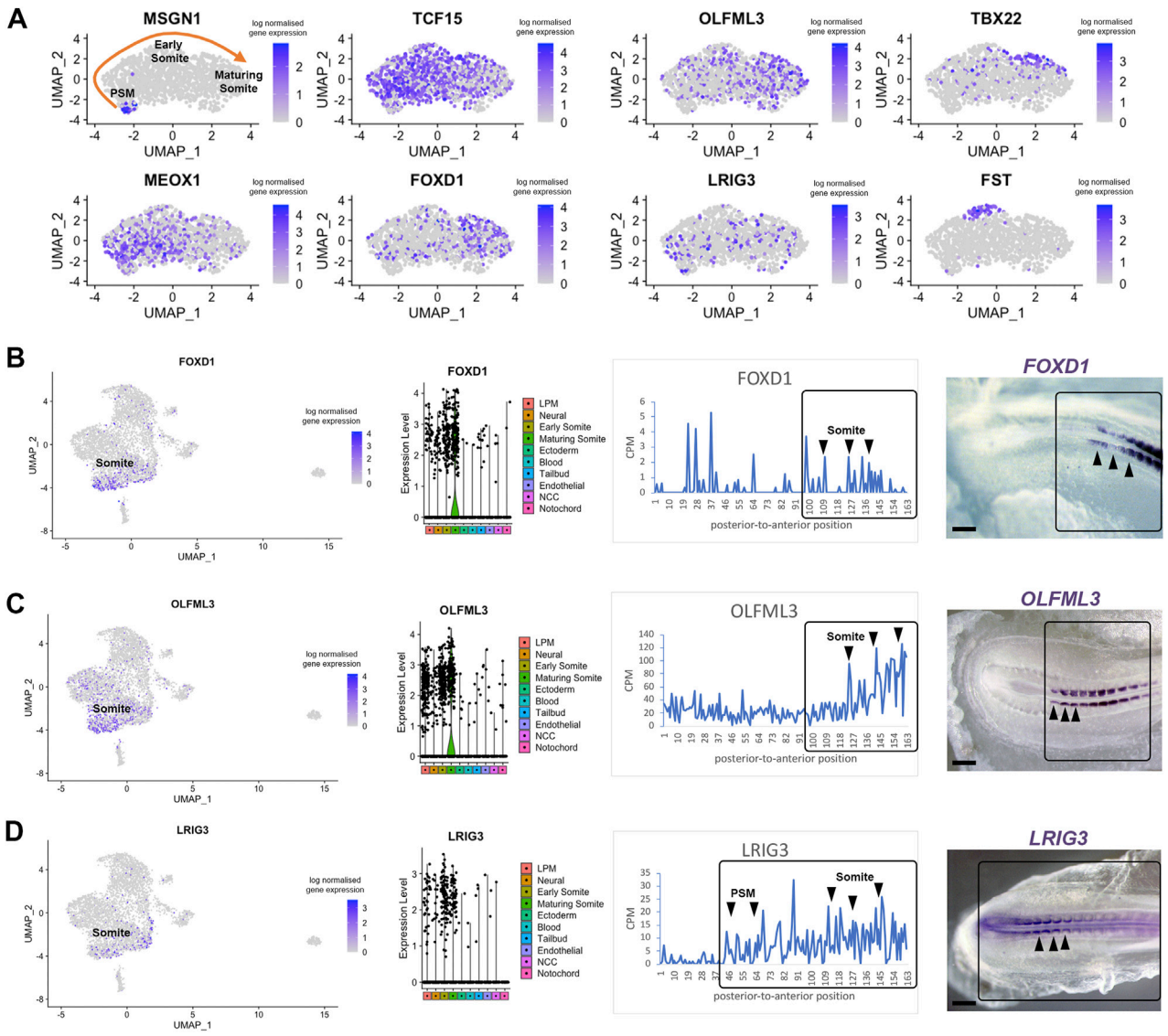


FIGURE 5
Differentially expressed genes in pre-somitic mesoderm and somites. **(A)** Sub-clustering identifies specific genes within the psm, early somites and maturing somites. Psm is characterised by *MSGN1* expression while *Tcf15*, *Meox1* and *Tbx22* markers represent somites. Restricted *Fst* expression may correlate with epaxial myoblasts. **(B–D)** UMAP, violin plots and spatial expression traces show expression for *Foxd1*, *Olfml3* and *Lrig3*, not previously identified in somites. The colour coding in the violin plots corresponds to the clusters identified in the scRNA-seq. Violin plots show higher levels of expression in maturing somites for *Foxd1* and *Olfml3* and a broader distribution for *Lrig3*. Whole mount *in situ* hybridisation confirmed the spatially restricted expression of *Foxd1* and *Olfml3* in epithelial and maturing somites and of *Lrig3* in the psm and somites.

## Discussion

The chick embryo is a classic model for developmental biology studies due to the versatility of *in vivo* experimental approaches (Stern, 2005; Sauka-Spengler and Barembaum, 2008; Gandhi and Bronner, 2018). For example, it has served to better understand the processes of body axis formation, segmentation/somitogenesis and differentiation (Benazeraf and Pourquie, 2013). Here we use single cell transcriptomics and RNA-tomography spatial transcriptomics to map cells that arise in the emerging trunk as it extends. This adds to the growing body of literature, which includes scRNA-seq data of the chick embryo from primitive streak to neurula stages (Vermillion et al., 2018; Williams et al., 2022). Previous work from other labs characterised the molecular signature of neuromesodermal progenitors (NMP) in detail by micro-dissecting anterior PS in stage HH5 and in 6-somite embryos (HH9$^-$) as well as the tail bud of 35-somite embryos (~HH18) (Guillot et al., 2021). We did not detect NMPs, which are characterised by co-expression of *T-brachyury* and *Sox2* (Wilson et al., 2009; Henrique et al., 2015; Wymeersch et al., 2021), as a discreet population. This is most likely due to the number of cells sequenced. A recent report examined the anterior most part of the main body axis, including occipital and cervical somites at several stages of development, 4-somites, 7-somites, 10-somites and 13-somites (Rito et al., 2023). This scRNA-seq data identified similar cell populations when the body extends and the cervical-thoracic

region forms (HH14, 22-somite embryo) and is in agreement with our data presented here.

Furthermore, we show that a combined analysis of scRNA-seq data with RNA-tomography spatial transcriptomics can reveal novel genes involved in specific aspects of axis extension. As an example, we focused on paraxial mesoderm and discovered the previously unknown relevance of *Foxd1*, *Olfml3* and *Lrig3* in developing somites. All three genes showed restricted expression in the medial somite domain suggesting a possible role in early myoblasts, however, this remains to be confirmed with functional approaches, such as gain- and loss-of function experiments. It is noteworthy that *Foxd1*, a member of the fork-head family of transcription factors, is associated with pluripotency and seems to be required for successful reprogramming (Koga et al., 2014). In addition, *Foxd1* protects senescence in human mesenchymal stem cells (hMSC) and is regulated by YAP (Fu et al., 2019). Interestingly, RNA-tomography line graphs indicated *Foxd1* expression peaks posteriorly, where progenitors reside. However, this was not confirmed by *in situ* hybridisation. The reason for this is unclear and could be due to the sensitivity of those different approaches. Not much is known about *Olfml3* function in development. It is a secreted glycoprotein of the Olfactomedin-family, which organises the extracellular matrix and has pro-angiogenic properties. *Olfml3* deficient mice exhibit abnormalities in the vasculature causing lethality (Imhof et al., 2020). *Olfml3* has also been implicated in pre-natal muscle development in pig (Jin and Li, 2019) and in *Xenopus* it is involved in dorso-ventral patterning by enhancing chordin degradation (Inomata et al., 2008). Finally, Leucine-rich repeats and immunoglobulin-like domains 3 (*Lrig3*) plays a role in neural crest development (Zhao et al., 2008) in *Xenopus*. This is consistent with studies in mice, which showed *Lrig3* is involved in inner ear morphogenesis by restricting the expression of *Ntn1* (Abraira et al., 2008). However, the roles of these genes in developing somites have not yet been investigated.

RNA-tomography is a spatial transcriptomics approach first used in zebrafish embryos (Junker et al., 2014; Kruse et al., 2016). We modified and automated the approach using the G&T-seq protocol (Macaulay et al., 2015) and applied it to the posterior half of a HH14 whole embryo, along the main body axis dimension. As reported previously in the zebrafish heart (Wu et al., 2016; Burkhard and Bakkers, 2018), we obtained high spatial resolution and sensitivity as shown by hierarchical cluster analysis. Known marker genes were expressed in the anticipated spatio-temporal patterns and identified the appropriate regions along the body axis. The extraembryonic tissue was characterized by *Hbm*, *Hbz*, *Lmo2* and *Epas1*, the tailbud region by *Hoxa13*, *Wnt5A*, the presegemented mesoderm by *Msgn1*, *Tbx6* and epithelial somites by *Meox1* and genes involved in retinoic acid (RA) signalling.

This study combines scRNA-seq with spatial information from RNA-tomography improving our understanding and validating the gene expression patterns within the avian elongating body axis and tailbud. While the scRNA-seq provides information on gene expression at the single-cell level, combining it with RNA-tomography bulk sequencing of cryosections allows preservation of the spatial context of gene activity along the anterior-posterior axis. Other technologies are now available for obtaining high-resolution spatial transcriptional profiles of tissues, such as MERFISH, 10X Genomics Visium and Xenium, although these also do not necessarily capture cellular resolution or multiple axial dimensions. Furthermore, all these approaches are more costly to implement, specifically with multiple samples as used here to reveal gene dynamics along the anterior-to-posterior axis. Overall, our results illustrate how combining different approaches can be advantageous when addressing fundamental questions in embryonic development.

# Materials and methods

## Chicken embryos

Fertilised chicken eggs (Henry Stewart & Co.) were incubated at 37°C with humidity. Embryos were staged according to (Hamburger and Hamilton, 1992). All experiments were performed on chicken embryos younger than two-thirds of gestation and therefore were not regulated by the Animal Scientific Procedures Act 1986.

## Preparation of single cells from chicken embryos

The trunk of HH14 embryos were dissected into Ringer's solution in silicon lined petri dishes and pinned down using the extra-embryonic membranes. Embryonic tissue was transferred into low binding tubes and Ringer's solution was replaced with Dispase (1.5 mg/mL) in DMEM 10 mM HEPES pH7.5 at 37°C for 7 min prior to treatment with Trypsin (0.05%) at 37°C for 7 min. The reaction was stopped with Ringer's solution with 0.25% BSA. Cells were spun down and resuspended in Hank's solution prior to passing through 40 µm cell strainer to obtain single cell suspension.

## scRNA-seq library preparation

A suspension of approximately 10,000 single cells was loaded onto the 10X Genomics Single Cell 3′ Chip. cDNA synthesis and library construction were performed according to the manufacturer's protocol for the Chromium Single Cell 3′ v2 protocol (PN-12033, 10X Genomics). Samples were sequenced on Illumina HiSeq 4,000 100 bp paired-end runs.

## scRNA-seq data analysis

Cell Ranger 3.0.2 (10X Genomics) was used to de-multiplex Illumina BCL output, create fastq files and generate single cell feature counts for the library using the *Gallus gallus* transcriptome (Ensembl release 94) with 82.4% reads mapped to the genome. Subsequent processing was performed using the Seurat v3.1.0 (Butler et al., 2018) package within R (v3.6.1). Cell quality was assessed using simple QC metrics: total number of expressed genes, mitochondrial RNA content and ribosomal RNA content. Identification of chicken mitochondrial RNA content and ribosomal RNA content. Outlier cells were identified if they were above or below three median absolute

deviations (MADs) from the median for any metric in the dataset. Data was normalised across all cells using the "LogNormalize" function with a scale factor of 1e4. A set of genes highly variable across the cells was identified using the 'FindVariableGenes' function (using "vst" and 2000 features) before being centred and scaled using the "ScaleData" function with default parameters. PCA analysis was performed on scaled data using variant genes and significant principal components were identified by plotting the standard deviation of the top 50 components. The first 2 principal components showed high enrichment for mitochondrial genes and were subsequently regressed and only principal components 3:25 were used to create a Shared Nearest Neighbour (SNN) graph using the "FindNeighbours" function with k.param set to 10. This was used to identify clusters of cells showing similar expression profiles using the FindClusters function with a resolution set to 0.6. The Uniform Manifold Approximation and Projection (UMAP) dimensional reduction technique was used to visualise data from principal components 3:26 in two-dimensional space ("RunUMAP" function). Graphing of the output enabled visualisation of cell cluster identity and marker gene expression. Biomarkers of each cluster were identified using Wilcoxon rank sum tests using Seurat's "FindAllMarkers" function. It was stipulated that genes must show a logFC of at least 0.01 to be considered for testing. Only positive markers were reported. The expression profile of top markers ranked by average logFC were visualised as heatmaps and dotplots of the scaled data. Cluster identity was determined using visual inspection focussing on the expression of known marker genes. For cells identified in tailbud and somite clusters, the "Subset" function was used to create a new Seurat object which narrowed down to 1,359 cells. Using the "FindNeighbors" feature with dimensions set to 3:20, "FindClusters" resolution of 0.4 and "RunUMAP" set with dimensions 3:16.

## RNA sequencing from serial sections—RNA-tomography

Embryos were embedded in Jung tissue freezing medium (Leica), orientated and rapidly frozen on dry ice, and stored at −80°C prior to cryosectioning. Embedded embryos were cryosectioned at 20 µm thickness, collected into 96-well plates (on ice) prior to the addition of 10 µL of RLT plus lysis buffer (Qiagen, Hilden, Germany). All instruments and surfaces were cleaned with 80% v/v ethanol, RNAse-free water and lastly RNAse-out solution after each sample to reduce cross-contamination and RNA degradation. Samples were stored at −80°C until cDNA preparation using the G&T-seq method as previously described (Macaulay et al., 2015) with minor modifications to accommodate the larger volume of lysis buffer. The polyA mRNA capture step of the G&T-seq protocol was used, which enables automated and parallel capture and amplification of RNA from serial sections. The genomic DNA component was not analysed in this study. cDNA was normalised to 0.2 ng/µL before Nextera (Illumina, San Diego, CA, United States) library preparation in a total reaction volume of 4 µL. Libraries were pooled by volume and sequenced on a single lane on the Illumina HiSeq 2,500 (150-bp paired-end reads).

## Low-input RNA sequencing analysis

For RNA-seq analysis, we used Refseq version GRCg6a for genome assembly and gene annotation. Reads were trimmed and adapters were removed using tim-galore version 0.4.2. Heatmap based on hierarchical clustering was generated in R-Studio version 1.2.1335 and plotted as a heatmap using the R package DeSeq2 (Love et al., 2014).

## Whole mount *in situ* hybridisation

Whole mount *in situ* hybridisation using DIG-UTP labelled antisense RNA probes was carried out using standard methods. Probes were generated from amplificons of chicken cDNA using the following primers: *Wnt5a* (GCAGCACTGTGGACAACAAC/CAC CGTCTTGAACTGGTCGT), *Olfml3* (GGGAGTTCACGCTCTTCT CG/GATGATCTGGTAGCCGTCGT) *Hbm* (CATCACACATTG CCACCAG C/GCAGCAATGGTGTCTTTATTGA), *Tbx22* (GGA TGTTCCCATCGGTCAGG/AGACTTAGCGCTCTT CAGGC), *Lrig3* (GTCCTGACGCCTGGGAATTT/AATCTGTGGGACAGG ATGCC), *Foxd1* (CCCGC ATCTCTAACTGTTAAGGG/ATTAAC CCTCACTAAAGGTCCCTCAAGCCTTCTCTGTTC). Briefly, following fixation in 4% PFA embryos were treated with Proteinase K, hybridised with the probe over night at 65°C. After post-hybridisation washed and blocking with BMB (Roche), embryos were treated with anti-DIG antibody coupled to alkaline phosphatase (Merck) and signal developed using NBT/BCIP (Melfords Laboratories).

# Data availability statement

The data presented in the study are deposited in the European Nucleotide Archive repository, accession number PRJEB74465 https://www.ebi.ac.uk/ena/browser/view/PRJEB74465.

# Ethics statement

The animal study was approved by the AWERB—Animal Welfare and Ethical Review Body. The study was conducted in accordance with the local legislation and institutional requirements.

# Author contributions

GM: Conceptualization, Formal Analysis, Investigation, Validation, Visualization, Writing–original draft, Writing–review and editing. ST: Investigation, Writing–review and editing. ES: Investigation, Validation, Writing–review and editing. LM: Investigation, Writing–review and editing. AL: Investigation, Writing–review and editing. JL: Investigation, Writing–review

and editing. VU: Data curation, Formal Analysis, Writing–review and editing. WH: Conceptualization, Data curation, Formal Analysis, Funding acquisition, Supervision, Writing–review and editing. IM: Conceptualization, Funding acquisition, Investigation, Supervision, Writing–review and editing. AM: Conceptualization, Funding acquisition, Project administration, Supervision, Writing–original draft, Writing–review and editing.

## Funding

The author(s) declare that financial support was received for the research, authorship, and/or publication of this article. The authors acknowledge support from the Biotechnology and Biological Sciences Research Council (BBSRC), part of UK Research and Innovation, BBSRC Core Strategic Programme Grant (Genomes to Food Security) BB/CSP1720/1 and the National Capability BBS/E/T/000PR9816 (NC1—Supporting EI's ISPs and the UK Community with Genomics and Single Cell Analysis). WH was additionally supported by the BBSRC Grant BBS/E/T/000PR9818. IM was supported by a BBSRC New Investigator Grant BB/P022073/1. ST was supported by the JIC/NRP International Undergraduate Summer School programme. AM acknowledges BBSRC funding (BB/N007034/1) and a NRPDTP studentship for ES.

## Conflict of interest

The authors declare that the research was conducted in the absence of any commercial or financial relationships that could be construed as a potential conflict of interest.

The author(s) declared that they were an editorial board member of Frontiers, at the time of submission. This had no impact on the peer review process and the final decision.

## Publisher's note



## Supplementary material

The Supplementary Material for this article can be found online at: https://www.frontiersin.org/articles/10.3389/fcell.2024.1382960/full#supplementary-material

## References

Abraira, V. E., Del Rio, T., Tucker, A. F., Slonimsky, J., Keirnes, H. L., and Goodrich, L. V. (2008). Cross-repressive interactions between Lrig3 and netrin 1 shape the architecture of the inner ear. *Development* 135, 4091–4099. doi:10.1242/dev.029330

Anderson, C., Hill, B., Lu, H. C., Moverley, A., Yang, Y., Oliveira, N. M. M., et al. (2019). A 3D molecular atlas of the chick embryonic heart. *Dev. Biol.* 456, 40–46. doi:10.1016/j.ydbio.2019.07.003

Baranski, M., Berdougo, E., Sandler, J. S., Darnell, D. K., and Burrus, L. W. (2000). The dynamic expression pattern of frzb-1 suggests multiple roles in chick development. *Dev. Biol.* 217, 25–41. doi:10.1006/dbio.1999.9516

Bell, G. W., Yatskievych, T. A., and Antin, P. B. (2004). GEISHA, a whole-mount *in situ* hybridization gene expression screen in chicken embryos. *Dev. Dyn.* 229, 677–687. doi:10.1002/dvdy.10503

Benazeraf, B., and Pourquie, O. (2013). Formation and segmentation of the vertebrate body axis. *Annu. Rev. Cell. Dev. Biol.* 29, 1–26. doi:10.1146/annurev-cellbio-101011-155703

Berti, F., Nogueira, J. M., Wohrle, S., Sobreira, D. R., Hawrot, K., and Dietrich, S. (2015). Time course and side-by-side analysis of mesodermal, pre-myogenic, myogenic and differentiated cell markers in the chicken model for skeletal muscle formation. *J. Anat.* 227, 361–382. doi:10.1111/joa.12353

Bhattacharyya, S., Bailey, A. P., Bronner-Fraser, M., and Streit, A. (2004). Segregation of lens and olfactory precursors from a common territory: cell sorting and reciprocity of Dlx5 and Pax6 expression. *Dev. Biol.* 271, 403–414. doi:10.1016/j.ydbio.2004.04.010

Brent, A. E., and Tabin, C. J. (2002). Developmental regulation of somite derivatives: muscle, cartilage and tendon. *Curr. Opin. Genet. Dev.* 12, 548–557. doi:10.1016/s0959-437x(02)00339-8

Burkhard, S. B., and Bakkers, J. (2018). Spatially resolved RNA-sequencing of the embryonic heart identifies a role for Wnt/β-catenin signaling in autonomic control of heart rate. *Elife* 7, e31515. doi:10.7554/eLife.31515

Butler, A., Hoffman, P., Smibert, P., Papalexi, E., and Satija, R. (2018). Integrating single-cell transcriptomic data across different conditions, technologies, and species. *Nat. Biotechnol.* 36, 411–420. doi:10.1038/nbt.4096

Cauthen, C. A., Berdougo, E., Sandler, J., and Burrus, L. W. (2001). Comparative analysis of the expression patterns of Wnts and Frizzleds during early myogenesis in chick embryos. *Mech. Dev.* 104, 133–138. doi:10.1016/s0925-4773(01)00369-0

Christ, B., Huang, R., and Scaal, M. (2007). Amniote somite derivatives. *Dev. Dyn.* 236, 2382–2396. doi:10.1002/dvdy.21189

Christ, B., and Scaal, M. (2008). Formation and differentiation of avian somite derivatives. *Adv. Exp. Med. Biol.* 638, 1–41. doi:10.1007/978-0-387-09606-3_1

Dubrulle, J., McGrew, M. J., and Pourquie, O. (2001). FGF signaling controls somite boundary position and regulates segmentation clock control of spatiotemporal Hox gene activation. *Cell.* 106, 219–232. doi:10.1016/s0092-8674(01)00437-8

Filipe, M., Goncalves, L., Bento, M., Silva, A. C., and Belo, J. A. (2006). Comparative expression of mouse and chicken Shisa homologues during early development. *Dev. Dyn.* 235, 2567–2573. doi:10.1002/dvdy.20862

Fu, L., Hu, Y., Song, M., Liu, Z., Zhang, W., Yu, F. X., et al. (2019). Up-regulation of FOXD1 by YAP alleviates senescence and osteoarthritis. *PLoS Biol.* 17, e3000201. doi:10.1371/journal.pbio.3000201

Gandhi, S., and Bronner, M. E. (2018). Insights into neural crest development from studies of avian embryos. *Int. J. Dev. Biol.* 62, 183–194. doi:10.1387/ijdb.180038sg

Griffiths, J. A., Scialdone, A., and Marioni, J. C. (2018). Using single-cell genomics to understand developmental processes and cell fate decisions. *Mol. Syst. Biol.* 14, e8046. doi:10.15252/msb.20178046

Gros, J., Scaal, M., and Marcelle, C. (2004). A two-step mechanism for myotome formation in chick. *Dev. Cell.* 6, 875–882. doi:10.1016/j.devcel.2004.05.006

Guillot, C., Djeffal, Y., Michaut, A., Rabe, B., and Pourquie, O. (2021). Dynamics of primitive streak regression controls the fate of neuromesodermal progenitors in the chicken embryo. *Elife* 10, e64819. doi:10.7554/eLife.64819

Hamburger, V., and Hamilton, H. L. (1992). A series of normal stages in the development of the chick embryo. 1951. *Dev. Dyn.* 195, 231–272. doi:10.1002/aja.1001950404

Henrique, D., Abranches, E., Verrier, L., and Storey, K. G. (2015). Neuromesodermal progenitors and the making of the spinal cord. *Development* 142, 2864–2875. doi:10.1242/dev.119768

Ibarra-Soria, X., Thierion, E., Mok, G. F., Munsterberg, A. E., Odom, D. T., and Marioni, J. C. (2023) *A transcriptional and regulatory map of mouse somitogenesis.*

Iimura, T., Yang, X., Weijer, C. J., and Pourquie, O. (2007). Dual mode of paraxial mesoderm formation during chick gastrulation. *Proc. Natl. Acad. Sci. U. S. A.* 104, 2744–2749. doi:10.1073/pnas.0610997104

Imhof, B. A., Ballet, R., Hammel, P., Jemelin, S., Garrido-Urbani, S., Ikeya, M., et al. (2020). Olfactomedin-like 3 promotes PDGF-dependent pericyte proliferation and migration during embryonic blood vessel formation. *FASEB J.* 34, 15559–15576. doi:10.1096/fj.202000751RR

Inomata, H., Haraguchi, T., and Sasai, Y. (2008). Robust stability of the embryonic axial pattern requires a secreted scaffold for chordin degradation. *Cell.* 134, 854–865. doi:10.1016/j.cell.2008.07.008

Jaffredo, T., Bollerot, K., Sugiyama, D., Gautier, R., and Drevon, C. (2005). Tracing the hemangioblast during embryogenesis: developmental relationships between endothelial and hematopoietic cells. *Int. J. Dev. Biol.* 49, 269–277. doi:10.1387/ijdb.041948tj

Javerzat, S., Franco, M., Herbert, J., Platonova, N., Peille, A. L., Pantesco, V., et al. (2009). Correlating global gene regulation to angiogenesis in the developing chick extra-embryonic vascular system. *PLoS One* 4, e7856. doi:10.1371/journal.pone.0007856

Jin, Y., and Li, J. L. (2019). Olfactomedin-like 3: possible functions in embryonic development and tumorigenesis. *Chin. Med. J. Engl.* 132, 1733–1738. doi:10.1097/CM9.0000000000000309

Joshi, P., Darr, A. J., and Skromne, I. (2019). CDX4 regulates the progression of neural maturation in the spinal cord. *Dev. Biol.* 449, 132–142. doi:10.1016/j.ydbio.2019.02.014

Junker, J. P., Noel, E. S., Guryev, V., Peterson, K. A., Shah, G., Huisken, J., et al. (2014). Genome-wide RNA Tomography in the zebrafish embryo. *Cell.* 159, 662–675. doi:10.1016/j.cell.2014.09.038

Koga, M., Matsuda, M., Kawamura, T., Sogo, T., Shigeno, A., Nishida, E., et al. (2014). Foxd1 is a mediator and indicator of the cell reprogramming process. *Nat. Commun.* 5, 3197. doi:10.1038/ncomms4197

Kruse, F., Junker, J. P., van Oudenaarden, A., and Bakkers, J. (2016). Tomo-seq: a method to obtain genome-wide expression data with spatial resolution. *Methods Cell. Biol.* 135, 299–307. doi:10.1016/bs.mcb.2016.01.006

Lobjois, V., Benazeraf, B., Bertrand, N., Medevielle, F., and Pituello, F. (2004). Specific regulation of cyclins D1 and D2 by FGF and Shh signaling coordinates cell cycle progression, patterning, and differentiation during early steps of spinal cord development. *Dev. Biol.* 273, 195–209. doi:10.1016/j.ydbio.2004.05.031

Macaulay, I. C., Haerty, W., Kumar, P., Li, Y. I., Hu, T. X., Teng, M. J., et al. (2015). G&T-seq: parallel sequencing of single-cell genomes and transcriptomes. *Nat. Methods* 12, 519–522. doi:10.1038/nmeth.3370

McColl, J., Mok, G. F., Lippert, A. H., Ponjavic, A., Muresan, L., and Munsterberg, A. (2018). 4D imaging reveals stage dependent random and directed cell motion during somite morphogenesis. *Sci. Rep.* 8, 12644. doi:10.1038/s41598-018-31014-3

McKeown, S. J., Lee, V. M., Bronner-Fraser, M., Newgreen, D. F., and Farlie, P. G. (2005). Sox10 overexpression induces neural crest-like cells from all dorsoventral levels of the neural tube but inhibits differentiation. *Dev. Dyn.* 233, 430–444. doi:10.1002/dvdy.20341

Minko, K., Bollerot, K., Drevon, C., Hallais, M. F., and Jaffredo, T. (2003). From mesoderm to blood islands: patterns of key molecules during yolk sac erythropoiesis. *Gene Expr. Patterns* 3, 261–272. doi:10.1016/s1567-133x(03)00053-x

Mok, G. F., Folkes, L., Weldon, S. A., Maniou, E., Martinez-Heredia, V., Godden, A. M., et al. (2021). Characterising open chromatin in chick embryos identifies cis-regulatory elements important for paraxial mesoderm formation and axis extension. *Nat. Commun.* 12, 1157. doi:10.1038/s41467-021-21426-7

Moris, N., Martinez Arias, A., and Steventon, B. (2020). Experimental embryology of gastrulation: pluripotent stem cells as a new model system. *Curr. Opin. Genet. Dev.* 64, 78–83. doi:10.1016/j.gde.2020.05.031

Nielsen, C., Murtaugh, L. C., Chyung, J. C., Lassar, A., and Roberts, D. J. (2001). Gizzard formation and the role of Bapx1. *Dev. Biol.* 231, 164–174. doi:10.1006/dbio.2000.0151

Nimmagadda, S., Geetha Loganathan, P., Huang, R., Scaal, M., Schmidt, C., and Christ, B. (2005). BMP4 and noggin control embryonic blood vessel formation by antagonistic regulation of VEGFR-2 (Quek1) expression. *Dev. Biol.* 280, 100–110. doi:10.1016/j.ydbio.2005.01.005

Olivera-Martinez, I., and Storey, K. G. (2007). Wnt signals provide a timing mechanism for the FGF-retinoid differentiation switch during vertebrate body axis extension. *Development* 134, 2125–2135. doi:10.1242/dev.000216

Ota, K., Nagai, H., and Sheng, G. (2007). Expression and hypoxic regulation of hif1alpha and hif2alpha during early blood and endothelial cell differentiation in chick. *Gene Expr. Patterns* 7, 761–766. doi:10.1016/j.modgep.2007.05.007

Pourquie, O. (2004). The chick embryo: a leading model in somitogenesis studies. *Mech. Dev.* 121, 1069–1079. doi:10.1016/j.mod.2004.05.002

Psychoyos, D., and Stern, C. D. (1996). Fates and migratory routes of primitive streak cells in the chick embryo. *Development* 122, 1523–1534. doi:10.1242/dev.122.5.1523

Reijntjes, S., Stricker, S., and Mankoo, B. S. (2007). A comparative analysis of Meox1 and Meox2 in the developing somites and limbs of the chick embryo. *Int. J. Dev. Biol.* 51, 753–759. doi:10.1387/ijdb.072332sr

Riddle, R. D., Johnson, R. L., Laufer, E., and Tabin, C. (1993). Sonic hedgehog mediates the polarizing activity of the ZPA. *Cell.* 75, 1401–1416. doi:10.1016/0092-8674(93)90626-2

Rito, T., Libby, A. R. G., Demuth, M., and Briscoe, J. (2023) *Notochord and axial progenitor generation by timely BMP and NODAL inhibition during vertebrate trunk formation*. USA: bioRxiv.

Roy, P., Kumar, B., Shende, A., Singh, A., Meena, A., Ghosal, R., et al. (2013). A genome-wide screen indicates correlation between differentiation and expression of metabolism related genes. *PLoS One* 8, e63670. doi:10.1371/journal.pone.0063670

Sanaki-Matsumiya, M., Matsuda, M., Gritti, N., Nakaki, F., Sharpe, J., Trivedi, V., et al. (2022). Periodic formation of epithelial somites from human pluripotent stem cells. *Nat. Commun.* 13, 2325. doi:10.1038/s41467-022-29967-1

Sauka-Spengler, T., and Barembaum, M. (2008). Gain- and loss-of-function approaches in the chick embryo. *Methods Cell. Biol.* 87, 237–256. doi:10.1016/S0091-679X(08)00212-4

Schubert, F. R., Mootoosamy, R. C., Walters, E. H., Graham, A., Tumiotto, L., Munsterberg, A. E., et al. (2002). Wnt6 marks sites of epithelial transformations in the chick embryo. *Mech. Dev.* 114, 143–148. doi:10.1016/s0925-4773(02)00039-4

Shukunami, C., Takimoto, A., Miura, S., Nishizaki, Y., and Hiraki, Y. (2008). Chondromodulin-I and tenomodulin are differentially expressed in the avascular mesenchyme during mouse and chick development. *Cell. Tissue Res.* 332, 111–122. doi:10.1007/s00441-007-0570-8

Stern, C. D. (2005). The chick; a great model system becomes even greater. *Dev. Cell.* 8, 9–17. doi:10.1016/j.devcel.2004.11.018

Stockdale, F. E., Nikovits, W., Jr., and Christ, B. (2000). Molecular and cellular biology of avian somite development. *Dev. Dyn.* 219, 304–321. doi:10.1002/1097-0177(2000)9999:9999<::AID-DVDY1057>3.0.CO;2-5

Sweetman, D., Wagstaff, L., Cooper, O., Weijer, C., and Munsterberg, A. (2008). The migration of paraxial and lateral plate mesoderm cells emerging from the late primitive streak is controlled by different Wnt signals. *BMC Dev. Biol.* 8, 63. doi:10.1186/1471-213X-8-63

Tavares, A. T., Izpisuja-Belmonte, J. C., and Rodriguez-Leon, J. (2001). Developmental expression of chick twist and its regulation during limb patterning. *Int. J. Dev. Biol.* 45, 707–713.

Trevers, K. E., Lu, H. C., Yang, Y., Thiery, A. P., Strobl, A. C., Anderson, C., et al. (2023). A gene regulatory network for neural induction. *Elife* 12, e73189. doi:10.7554/eLife.73189

Turner, D. A., Girgin, M., Alonso-Crisostomo, L., Trivedi, V., Baillie-Johnson, P., Glodowski, C. R., et al. (2017). Anteroposterior polarity and elongation in the absence of extra-embryonic tissues and of spatially localised signalling in gastruloids: mammalian embryonic organoids. *Development* 144, 3894–3906. doi:10.1242/dev.150391

Veenvliet, J. V., Bolondi, A., Kretzmer, H., Haut, L., Scholze-Wittler, M., Schifferl, D., et al. (2020). Mouse embryonic stem cells self-organize into trunk-like structures with neural tube and somites. *Science* 370, eaba4937. doi:10.1126/science.aba4937

Veenvliet, J. V., and Herrmann, B. G. (2021). Modeling mammalian trunk development in a dish. *Dev. Biol.* 474, 5–15. doi:10.1016/j.ydbio.2020.12.015

Vermillion, K. L., Bacher, R., Tannenbaum, A. P., Swanson, S., Jiang, P., Chu, L. F., et al. (2018). Spatial patterns of gene expression are unveiled in the chick primitive streak by ordering single-cell transcriptomes. *Dev. Biol.* 439, 30–41. doi:10.1016/j.ydbio.2018.04.007

Weldon, S. A., and Munsterberg, A. E. (2022). Somite development and regionalisation of the vertebral axial skeleton. *Semin. Cell. Dev. Biol.* 127, 10–16. doi:10.1016/j.semcdb.2021.10.003

Williams, R. M., Lukoseviciute, M., Sauka-Spengler, T., and Bronner, M. E. (2022). Single-cell atlas of early chick development reveals gradual segregation of neural crest lineage from the neural plate border during neurulation. *Elife* 11, e74464. doi:10.7554/eLife.74464

Wilson, V., Olivera-Martinez, I., and Storey, K. G. (2009). Stem cells, signals and vertebrate body axis extension. *Development* 136, 1591–1604. doi:10.1242/dev.021246

Wu, C. C., Kruse, F., Vasudevarao, M. D., Junker, J. P., Zebrowski, D. C., Fischer, K., et al. (2016). Spatially resolved genome-wide transcriptional profiling identifies BMP signaling as essential regulator of zebrafish cardiomyocyte regeneration. *Dev. Cell.* 36, 36–49. doi:10.1016/j.devcel.2015.12.010

Wymeersch, F. J., Wilson, V., and Tsakiridis, A. (2021). Understanding axial progenitor biology *in vivo* and *in vitro*. *Development* 148, dev180612. doi:10.1242/dev.180612

Xiong, F., Ma, W., Benazeraf, B., Mahadevan, L., and Pourquie, O. (2020). Mechanical coupling coordinates the Co-elongation of axial and paraxial tissues in avian embryos. *Dev. Cell.* 55, 354–366. doi:10.1016/j.devcel.2020.08.007

Yamanaka, Y., Hamidi, S., Yoshioka-Kobayashi, K., Munira, S., Sunadome, K., Zhang, Y., et al. (2023). Reconstituting human somitogenesis *in vitro*. *Nature* 614, 509–520. doi:10.1038/s41586-022-05649-2

Yanai, M., Tatsumi, N., Endo, F., and Yokouchi, Y. (2005). Analysis of gene expression patterns in the developing chick liver. *Dev. Dyn.* 233, 1116–1122. doi:10.1002/dvdy.20413

Yang, X., Dormann, D., Munsterberg, A. E., and Weijer, C. J. (2002). Cell movement patterns during gastrulation in the chick are controlled by positive and negative chemotaxis mediated by FGF4 and FGF8. *Dev. Cell.* 3, 425–437. doi:10.1016/s1534-5807(02)00256-3

Zhao, H., Tanegashima, K., Ro, H., and Dawid, I. B. (2008). Lrig3 regulates neural crest formation in Xenopus by modulating Fgf and Wnt signaling pathways. *Development* 135, 1283–1293. doi:10.1242/dev.015073

Zhou, Q., Choi, G., and Anderson, D. J. (2001). The bHLH transcription factor Olig2 promotes oligodendrocyte differentiation in collaboration with Nkx2.2. *Neuron* 31, 791–807. doi:10.1016/s0896-6273(01)00414-7